

A probable stellar solution to the cosmological lithium discrepancy

A.J. Korn¹, F. Grundahl², O. Richard³, P.S. Barklem¹, L. Mashonkina⁴, R. Collet¹, N. Piskunov¹ & B. Gustafsson¹

The measurement of the cosmic microwave background has strongly constrained the cosmological parameters of the Universe¹. When the measured density of baryons (ordinary matter) is combined with standard Big Bang nucleosynthesis calculations^{2,3}, the amounts of hydrogen, helium and lithium produced shortly after the Big Bang can be predicted with unprecedented precision^{1,4}. The predicted primordial lithium abundance is a factor of two to three higher than the value measured in the atmospheres of old stars^{5,6}. With estimated errors of 10 to 25 %, this cosmological lithium discrepancy seriously challenges our understanding of stellar physics, Big Bang nucleosynthesis or both. Certain modifications to nucleosynthesis have been proposed⁷, but found experimentally not to be viable⁸. Diffusion theory, however, predicts atmospheric abundances of stars to vary with time⁹, which offers a possible explanation of the discrepancy. Here we report spectroscopic observations of stars in the metal-poor globular cluster NGC 6397 that reveal trends of atmospheric abundance with evolutionary stage for various elements. These element-specific trends are reproduced by stellar-evolution models with diffusion and turbulent mixing¹⁰. We thus conclude that diffusion is predominantly responsible for the low apparent stellar lithium abundance in the atmospheres of old stars by transporting the lithium deep into the star.

Diffusive processes altering the elemental composition in stars have been studied for decades^{9,11}. Evidence for their importance comes from helioseismology¹² and the study of hot stars with peculiar abundance patterns¹³. Among solar-type

stars, the effects of diffusion are expected to be more pronounced in old, very metal-poor stars. Given their greater age, diffusion has had more time to produce sizeable effects than in younger stars like the Sun. Detailed element-by-element predictions from models including effects of atomic diffusion and radiative accelerations became available a few years ago¹⁴, but these early models produced strong abundance trends that are incompatible with measurements of, in particular, the abundance of lithium common among stars of the Galactic halo over a wide range of metallicities (the so-called Spite plateau of lithium). However, the recent inclusion of turbulent mixing¹⁰ brings model predictions into better agreement with observations.

According to the predictions from such model calculations, stars leaving the main-sequence (turn-off stars) are expected to show the largest variations relative to the composition of the gas from which the stars originated. Giant stars, however, have deep surface convection zones which erase most effects of diffusion and restore the original composition. One notable exception is lithium which disintegrates in layers with $T \geq 2.1$ million K. The destruction of lithium inside the star leads to a successive dilution of the surface lithium because the convective envelope expands when the star becomes a red giant. We performed spectroscopic observations specifically to test these model predictions.

Globular-cluster stars have identical age and initial heavy-element composition, and thus measured atmospheric abundance trends with evolutionary stage are a signature of diffusion. We observed 18 stars along the evolutionary sequence of NGC 6397 with the multi-object spectrograph FLAMES-UVES on the 8.2-m Very Large Telescope in Chile – five stars close to the main-sequence turn-off point (TOP), two stars in the middle of the subgiant branch (SGB), five stars at the base of the red-giant branch (bRGB) and six red giants (RGB) – that represent specific stages in stellar evolution (Fig. 2). Even on 8-m-class telescopes, these observations are still challenging, requiring total integration times of 2–12 hours per star to obtain homogeneous data with high signal-to-noise ratios at high spectral resolution.

These observational challenges explain in part why there have been surprisingly few studies looking for abundance trends between unevolved and evolved stars in globular clusters. One study¹⁵ found lower abundances for subgiants in the very metal-poor globular cluster M 92 than accepted literature values

¹Department of Astronomy and Space Physics, Uppsala University, Box 515, 75120 Uppsala, Sweden.

²Department of Physics and Astronomy, University of Århus, Ny Munkegade, 8000 Århus C, Denmark.

³3GRAAL-UMR5024/ISTEEM (CNRS), Université Montpellier II, Place E. Bataillon, 34095 Montpellier, France.

⁴Institute of Astronomy, Russian Academy of Science, Pyatnitskaya 48, 119017 Moscow, Russia.

Mean stellar parameters, iron abundances and photometric quantities of the four groups of stars

Group	No. of star	T_{eff} (K)	$\log [g \text{ (cm s}^{-2}\text{)}]$	$\log[\varepsilon \text{ (Fe)}]$	$\xi \text{ (km s}^{-1}\text{)}$
TOP	5	6254	3.89	5.23 ± 0.04	2.00
SGB	2	5805	3.58	5.27 ± 0.05	1.75
bRGB	5	5456	3.37	5.33 ± 0.03	1.73
RGB	6	5130	2.56	5.39 ± 0.02	1.60
Sun	1	5777	4.44	7.51	1.00
		$\Delta T_{\text{eff}} \text{ (TOP - RGB) (K)}$	$\Delta \log g \text{ (TOP - RGB)}$	$\Delta \log \varepsilon \text{ (Fe) (TOP - RGB)}$	
Spectroscopy		1124	1.33	0.16 ± 0.05	
Strömgren, ($v - y$)		1108	1.38	–	
Broad-band, ($V - I$)		1070	1.38	–	

Table 1: Mean stellar parameters of the four groups of stars in the following evolutionary stages: TOP, SGB, bRGB and RGB (see text). The FLAMES-UVES spectra cover the spectral range from 4800 - 6800 Å, have $R = \lambda/\Delta\lambda = 48\,000$ (where λ is wavelength) and signal-to-noise ratios in excess of 80:1 per pixel. The analyses are fully spectroscopic and line-by-line differential to the Sun. Typical errors on T_{eff} , $\log g$ and the microturbulence ξ for individual stars are, respectively, 150 K, 0.15 and 0.2 km s^{-1} . The errors in $\log[\varepsilon(\text{Fe})] = \log(N_{\text{Fe}}/N_{\text{H}}) + 12$ are the combined values of the line-to-line scatter of Fe I and Fe II for the individual stars propagated into the mean value for the group. Between 20 and 40 Fe I and Fe II lines were measured by means of profile fits. The stellar parameters of the TOP and SGB group have not been corrected for helium diffusion, which would result in higher $\log g$ values (+0.05; see text). Below, the spectroscopic results are compared with the photometry (Strömgren and broad-band indices calibrated on the infrared-flux method²⁸, see also Table 2) obtained with the Danish 1.54-m telescope on La Silla. In both cases, $\Delta \log g$ is based on the magnitude difference in V .

indicate for giant stars. However, the low signal-to-noise data did not allow firm conclusions. A different study¹⁶ examined TOP stars and subgiant stars in NGC 6397. It concentrated on elements showing suspected nuclear processing (oxygen, sodium, magnesium and aluminium). The analysis was based on standard models of stellar evolution and spectroscopic analysis (assuming equilibrium) and did not indicate significant differences in iron abundances. This result critically depends on the above-mentioned assumptions, which yield stellar parameters (effective temperatures) unsupported by photometry. The only previous study attempting a homogeneous analysis of red-giant and dwarf stars¹⁷ targeted M 13, a globular cluster a factor of three more metal-rich than NGC 6397. The highest-gravity object (a subgiant with $\log g = 3.8$) indeed shows an iron abundance 41% (0.23 in log abundance) below the average of the other 24 more evolved cluster members analysed. This was not interpreted as an indication of departures from a uniform cluster composition as caused by diffusion.

To derive stellar parameters and elemental abundances from our observations, we employed well-established spectroscopic diagnostics (in one dimension) with a high level of modelling realism in the line formation

(non-equilibrium where necessary). The profile of the Balmer line of hydrogen ($H\alpha$, at 656 nm) was used to estimate the effective temperatures (T_{eff})^{18,19}, while the ionization equilibrium of iron (treated in non-equilibrium) was used to determine the stellar surface gravities ($\log g$)²⁰. The mean stellar parameters for the four groups of stars are given in Table 1.

An independent check of the reliability of the stellar-parameter determination is obtained based on photometry, exploiting the luminosity difference of the stars. These data are also given in Table 1. As can be seen, the spectroscopic ΔT_{eff} (TOP – RGB) (that is, $T_{\text{eff}}(\text{TOP}) - T_{\text{eff}}(\text{RGB})$) is well-matched by both the Strömgren index ($v - y$) and the broad-band index ($V - I$), the photometry indicating a ΔT_{eff} only 20-50 K (2-5%) lower. The spectroscopic $\Delta \log g$ (TOP – RGB) is only 0.05 below that determined from the photometry. This is excellent agreement for two fully independent methods and we thus consider the stellar-parameter differences to be well constrained. On the basis of these differences, relative abundance trends can be scrutinized.

The best-determined abundance (in terms of number of spectral lines used) is that of iron. We find the abundance to differ by 45% (0.16 in log abundance), that is, the TOP stars have the lowest abundance

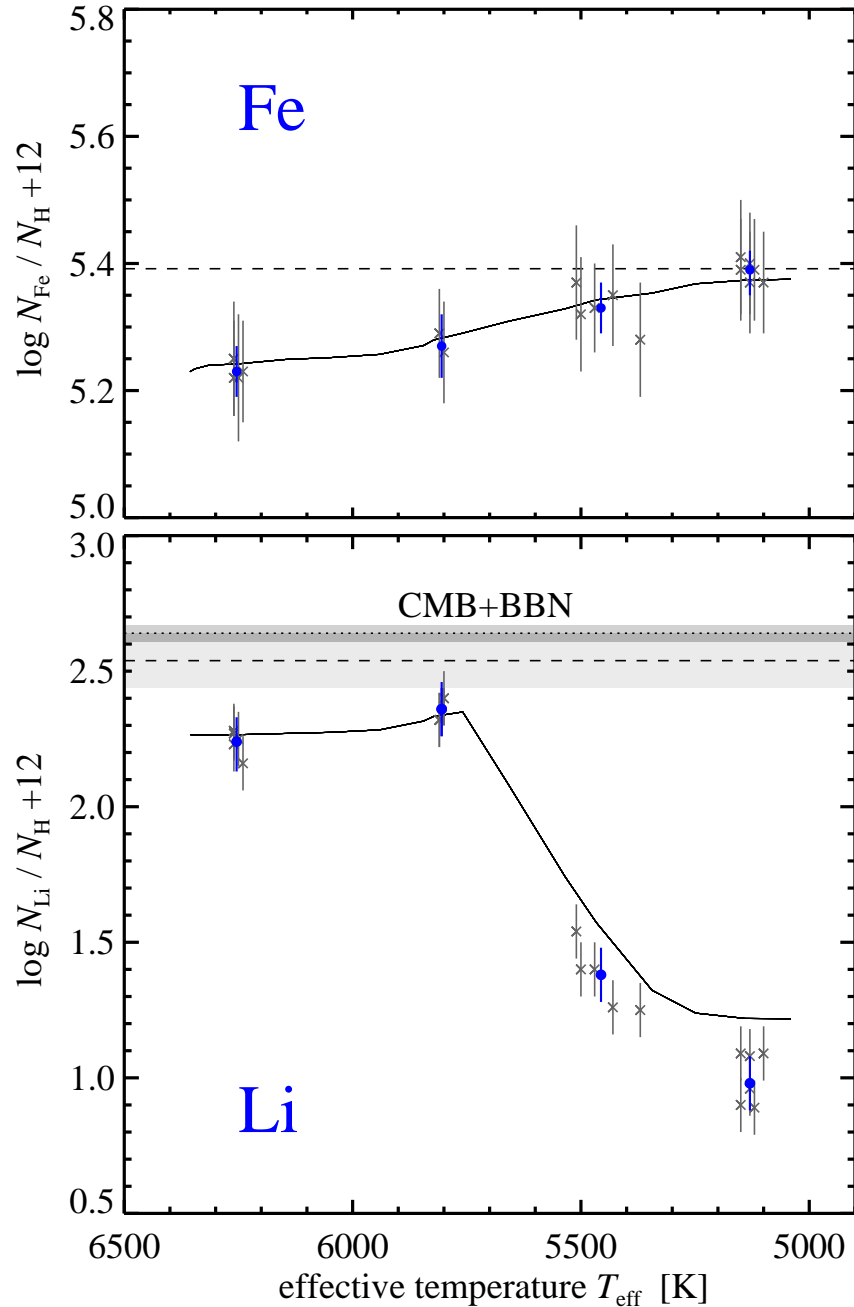


Figure 1: Trends of iron and lithium as a function of the effective temperatures of the observed stars compared to the model predictions. The grey crosses are the individual measurements, while the bullets are the group averages. The solid lines are the predictions of the diffusion model, with the original abundance given by the dashed line. In *b*, the grey-shaded area around the dotted line indicates the 1σ confidence interval of CMB + BBN¹: $\log[\varepsilon(\text{Li})] = \log(N_{\text{Li}}/N_{\text{H}}) + 12 = 2.64 \pm 0.03$. In *a*, iron is treated in non-equilibrium²⁰ (non-LTE), while in *b*, the equilibrium (LTE) lithium abundances are plotted, because the combined effect of 3D and non-LTE corrections was found to be very small²⁹. For iron, the error bars are the line-to-line scatter of Fe I and Fe II (propagated into the mean for the group averages), whereas for the absolute lithium abundances 0.10 is adopted. The 1σ confidence interval around the inferred primordial lithium abundance ($\log[\varepsilon(\text{Li})] = 2.54 \pm 0.10$) is indicated by the light-grey area. We attribute the modelling shortcomings with respect to lithium in the bRGB and RGB stars to the known need for extra mixing³⁰, which is not considered in the diffusion model.

which successively rises towards the RGB stars (Fig. 1a). Propagating the line-to-line scatter for all iron lines of each star into the mean values given in Table 1 and further into the abundance difference between TOP and RGB stars, the difference $\Delta \log \varepsilon(\text{Fe})$ (TOP – RGB) is significant at the 3.2σ level. Calcium and titanium also show trends (Fig. 3), but these are less pronounced.

We have compared these abundance trends with various diffusion model predictions and found that a model with one particular value of the turbulent-mixing efficiency¹⁰ is capable of fitting the observations of these heavy elements well. This model (model T6.0, with a parametric description of turbulent mixing using an isotropic turbulent diffusion coefficient 400 times larger than the atomic diffusion coefficient for helium at $\log T = 6.0$ varying with density as ρ^{-3} (ref. 10), and computed for the metallicity of the RGB stars) clearly predicts a steeper trend for iron than for calcium or titanium, in agreement with the observations. The simultaneous element-specific reproduction of the observations thus lends strong support for the diffusion interpretation of these trends and constrains the level of turbulent mixing.

We emphasize that it is not possible to remove all trends simultaneously by adjusting the stellar parameters: the neutral species Ca I and Fe I (both affected by non-equilibrium) require a T_{eff} correction of roughly 100 K and 200 K respectively, while the ionized species Ti II and Fe II (formed in equilibrium) would require a change in $\log g$ of 0.15 and 0.33, respectively. Considering the agreement between spectroscopy and photometry, these corrections to the stellar parameters are large and incompatible with one another. We also investigate the effect that the three-dimensional (3D) hydrodynamic nature of stellar atmospheres²¹ might have on the observed trends. Using 3D TOP and RGB models available to us, we find that the trends inferred from weak Fe II and Ti II lines in one dimension require small 3D corrections only. For iron, the trend would even be slightly steeper. As the stellar-parameter differences are well determined, analyses based on 3D hydrodynamic models would reach much the same conclusion about the abundance trends.

In the light of the identified diffusion signature, we should consider the structural effect that helium diffusion has on the atmosphere and, therefore, on the spectroscopic analysis. The T6.0 model predicts the He/H ratio in the TOP stars to be decreased by nearly

50% from the original value, 40% in the SGB stars, whereas the original ratio is almost restored in the bRGB and RGB stars. Helium settling of this extent changes the mean molecular weight in the atmosphere appreciably, an effect which can be mapped as a shift in gravity²². The accompanying shift in $\log g$ amounts to +0.05 for both groups, bringing the spectroscopic $\Delta \log g$ (TOP – RGB) into perfect agreement with the photometry-based value. This correction also improves the agreement of the stellar parameters with the isochrone (Fig. 2).

Lithium is ionized easily and therefore behaves much like helium in terms of settling. As seen from Fig. 1b, both the TOP stars and the SGB stars sample the lithium plateau. The observations support the T6.0 model predictions, with a slight upturn towards cooler temperatures before the convection zone encompasses lithium-free layers and dilution sets in. A higher value of lithium among halo subgiants than among halo dwarf stars was recently reported²³ and qualitatively interpreted as a signature of atomic diffusion counterbalanced by gravity-wave-induced mixing. In quantitative terms, the diffusion model we use predicts the original lithium abundance to be 78% (0.25 in log abundance) higher than the mean value measured in the TOP and SGB stars. Therefore, we infer a primordial lithium abundance which agrees with the cosmic microwave background plus Big Bang nucleosynthesis (CMB + BBN) value¹ within the mutual 1σ error bars. Given the uncertainties associated with both values, the cosmological lithium discrepancy is thus largely removed. This finding restores confidence in standard BBN, quantitative spectroscopy and sophisticated stellar evolution models.

In extrapolating to the primordial lithium abundance, we do not consider corrections related to the Galactic chemical evolution of lithium. Such corrections are model-dependent and rather uncertain. It is plausible that some fraction of the halo gas was processed through Population III stars²⁴ (lowering the lithium abundance) and that cosmic rays interacting with the interstellar medium have produced some lithium⁶. At present it is, however, unclear to which extent (and even in which direction) the stellar lithium abundances should be adjusted.

While helium diffusion has been invoked to lower globular-cluster ages to values which meet the cosmological age constraint, metal diffusion has rarely been considered. The models including atomic diffusion, radiative accelerations and turbulent mixing for all

elements will result in moderately different absolute and relative ages. Using similar models²⁵, the analysis of M 92 has led to an age estimate compatible with Wilkinson Microwave Anisotropy Probe (WMAP¹) results. It is clear, however, that stellar-evolution models need to be developed further towards physical self-consistency with respect to all relevant processes, including hydrodynamics and rotation. In particular, the physical mechanism causing turbulent mixing should be identified. Promising work²⁶ points towards the importance of internal gravity waves in transporting angular momentum and mixing stellar interiors.

Regarding unevolved metal-poor stars as tracers of Galactic cosmochemistry, heavy-element abundance ratios (for example, Mg/Fe) are less affected by diffusion than ratios with respect to hydrogen (for example, Fe/H). However, the effects are non-negligible and must be taken into account to reach the highest accuracy. Care should be taken especially when comparing abundances from giant and dwarf stars. In this respect, one exceptional pair is the two most metal-poor stars known²⁷, whose abundance signatures will have to be reinvestigated in the light of diffusion.

Received 28 March; accepted 14 June 2006.

1. Spergel, D. N. et al. Wilkinson Microwave Anisotropy Probe (WMAP) three year results: implications for cosmology. *Astrophys. J.* (submitted); preprint at <http://arxiv.org/abs/astro-ph/0603449> (2006).
2. Wagoner, R. V., Fowler, W. A. & Hoyle, F. On the synthesis of elements at very high temperatures. *Astrophys. J.* 148, 3-49 (1967).
3. Burles, S., Nollett, K. M. & Turner, M. S. Big bang nucleosynthesis predictions for precision cosmology. *Astrophys. J.* 552, L1-L5 (2001).
4. Cyburt, R. H., Fields, B. D. & Olive, K. A. Primordial nucleosynthesis in light of WMAP. *Phys. Lett. B* 567, 227-234 (2003).
5. Spite, M. & Spite, F. Lithium abundance at the formation of the galaxy. *Nature* 297, 483-485 (1982).
6. Ryan, S. G., Norris, J. E. & Beers, T. C. The Spite lithium plateau: ultrathin but postprimordial. *Astrophys. J.* 523, 654-677 (1999).
7. Coc, A., Vangioni-Flam, E., Descouvemont, P., Adahchour, A. & Angulo, C. Updated big bang nucleosynthesis compared with Wilkinson Microwave Anisotropy Probe observations and the abundance of light elements. *Astrophys. J.* 600, 544-552 (2004).
8. Angulo, C. et al. The ${}^7\text{Be}(d,p)2\alpha$ cross section at big bang energies and the primordial ${}^7\text{Li}$ abundance. *Astrophys. J.* 630, L105-L108 (2005).
9. Aller, L. H. & Chapman, S. Diffusion in the sun. *Astrophys. J.* 132, 461-472 (1960).
10. Richard, O., Michaud, G. & Richer, J. Implications of WMAP observations on Li abundance and stellar evolution models. *Astrophys. J.* 619, 538-548 (2005).
11. Michaud, G., Fontaine, G. & Beaudet, G. The lithium abundance: constraints on stellar evolution. *Astrophys. J.* 282, 206-213 (1984).
12. Guzik, J. A. & Cox, A. N. On the sensitivity of high-degree p-mode frequencies to the solar convection zone helium abundance. *Astrophys. J.* 386, 729-733 (1992).
13. Richer, J., Michaud, G. & Turcotte, S. The evolution of AMFM stars, abundance anomalies, and turbulent transport. *Astrophys. J.* 529, 338-356 (2000).
14. Richard, O., Michaud, G. & Richer, J. Models of metal-poor stars with gravitational settling and radiative accelerations. III. Metallicity dependence. *Astrophys. J.* 580, 1100-1117 (2002).
15. King, J. R., Stephens, A., Boesgaard, A. M. & Deliyannis, C. Keck HIRES spectroscopy of M92 subgiants – surprising abundances near the turnoff. *Astron. J.* 115, 666-684 (1998).
16. Gratton, R. G. et al. The O-Na and Mg-Al anticorrelations in turn-off and early subgiants in globular clusters. *Astron. Astrophys.* 369, 87-98 (2001).
17. Cohen, J. G. & Melendez, J. Abundances in a large sample of stars in M3 and M13. *Astron. J.* 129, 303-329 (2005).
18. Fuhrmann, K., Axer, M. & Gehren, T. Balmer lines in cool dwarf stars. I. Basic influence of atmospheric models. *Astron. Astrophys.* 271, 451-462 (1993).
19. Barklem, P. S., Piskunov, N. & O'Mara, B. J. Self-broadening in Balmer line wing formation in stellar atmospheres. *Astron. Astrophys.* 363, 1091-1105 (2000).
20. Korn, A. J., Shi, J. & Gehren, T. Kinetic equilibrium of iron in the atmospheres of cool stars. III. The ionization equilibrium of selected reference stars. *Astron. Astrophys.* 407, 691-703 (2003).
21. Stein, R. F. & Nordlund, Å. Simulations of solar granulation. I. General properties. *Astrophys. J.* 499, 914-933 (1998).

22. Strömgren, B., Gustafsson, B. & Olsen, E. H. Evidence of helium abundance differences between the Hyades stars and field stars, and between Hyades stars and Coma cluster stars. *Astron. Soc. Pacif.* 94, 5-15 (1982).
23. Charbonnel, C. & Primas, F. The lithium content of the galactic halo stars. *Astron. Astrophys.* 442, 961-992 (2005).
24. Piau, L. et al. From first stars to the Spite plateau: a possible reconciliation of halo stars observations with predictions from big bang nucleosynthesis. *Astrophys. J.* (submitted); preprint at <http://arxiv.org/abs/astro-ph/06035531> (2006).
25. Vandenberg, D. A., Richard, O., Michaud, G. & Richer, J. Models of metal-poor stars with gravitational settling and radiative accelerations. II. The age of the oldest stars. *Astrophys. J.* 571, 487-500 (2002).
26. Charbonnel, C. & Talon, S. Influence of gravity waves on the internal rotation and Li abundance of solar-type stars. *Science* 309, 2189-2191 (2005).
27. Frebel, A. et al. Nucleosynthetic signatures of the first stars. *Nature* 434, 871-873 (2005).
28. Alonso, A., Arribas, S. & Martinez-Roger, C. The effective temperature scale of giant stars (F0-K5). II. Empirical calibration of T_{eff} versus colours and [Fe/H]. *Astron. Astrophys. Suppl.* 140, 261-277 (1999).
29. Barklem, P. S., Belyaev, A. K. & Asplund, M. Inelastic $\text{H} + \text{Li}$ and $\text{H}^- + \text{Li}^+$ collisions and non-LTE Li I line formation in stellar atmospheres. *Astron. Astrophys.* 409, L1-L4 (2003).
30. Charbonnel, C. A consistent explanation for $^{12}\text{C}/^{13}\text{C}$, ^7Li and ^3He anomalies in red giant stars. *Astrophys. J.* 453, L41-L44 (1995).

providing colour-temperature relations specific to this project.

Author Information Reprints and permissions information is available at npg.nature.com/reprintsandpermissions. The authors declare no competing financial interests. Correspondence and requests for materials should be addressed to A.J.K. (akorn@astro.uu.se).

Supplementary Information is linked to the online version of the paper at www.nature.com/nature.

Acknowledgements A.J.K. acknowledges a research fellowship by the Leopoldina Foundation, Germany. O.R. thanks the Centre Informatique National de l'Enseignement Supérieur (CINES) and the Réseau Québécois de Calcul de Haute Performance (RQCHP) for providing the computational resources required for this work. F.G. acknowledges financial support from the Instrument Center for Danish Astrophysics (IDA). L.M. acknowledges support through the Presidium RAS Programme 'Origin and evolution of stars and the Galaxy'. The Uppsala group of authors acknowledges support from the Swedish Research Council. We thank A. Alonso and I. Ramirez for

Supplementary information

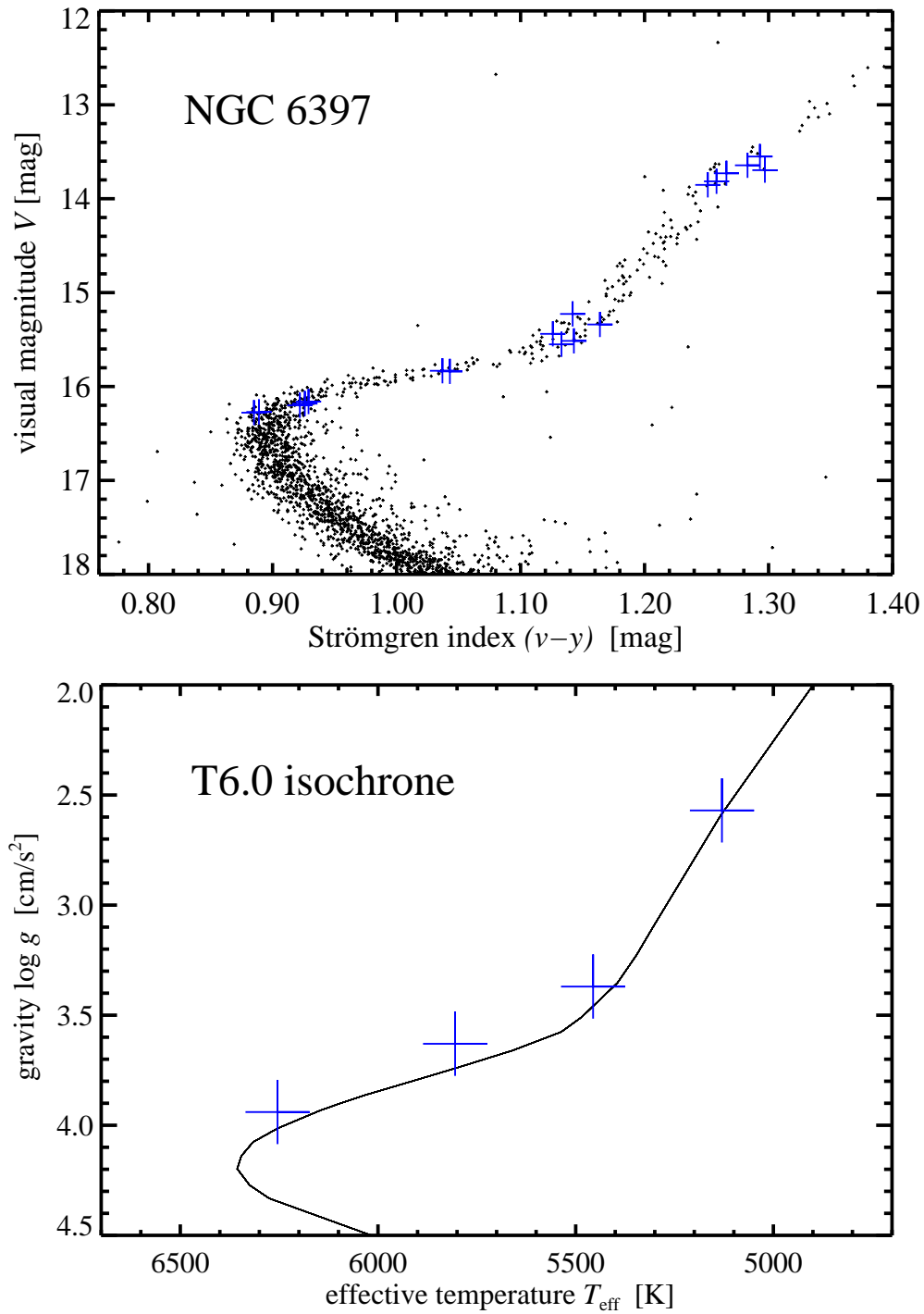


Figure 2: Loci of the observed stars in the observational and physical parameter space. *Top:* Colour-magnitude diagram of NGC 6397 clearly showing the main sequence, the subgiant branch and the red-giant branch. The observed stars are indicated by the blue crosses. *Bottom:* Comparison of the spectroscopic stellar parameters (corrected for helium diffusion, see text) with a 13.5 Gyr isochrone constructed from the diffusion model T6.0. The agreement is satisfactory indicating that the absolute stellar parameters meet the cosmological age constraint.

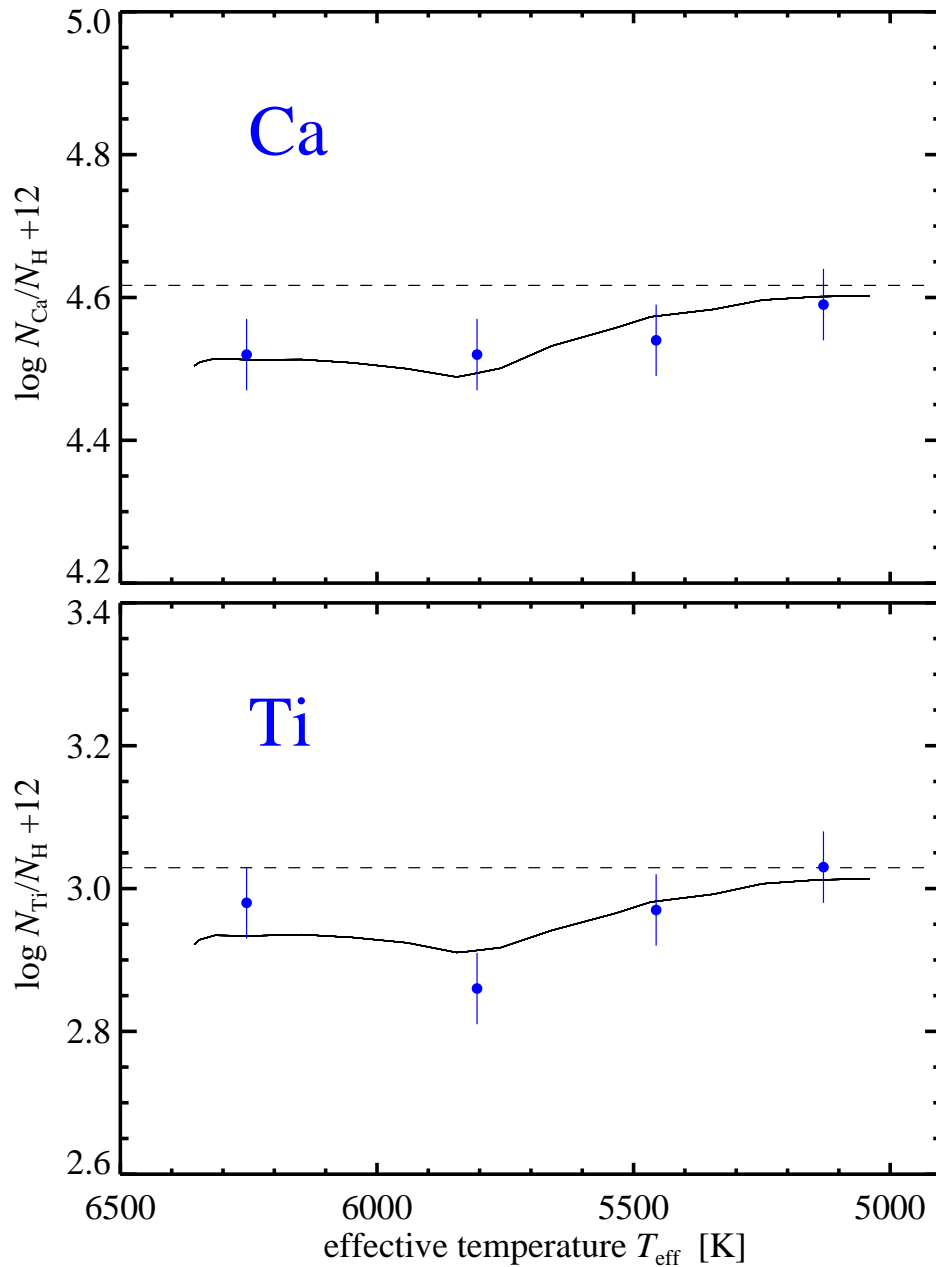


Figure 3: Trends of calcium and titanium as a function of the effective temperatures of the observed stars compared to the model predictions. As weak lines were used, the analyses were done on the mean spectra for each group of stars using the mean stellar parameters given in Table 1. The calcium abundances (*top*) were determined in non-LTE from three neutral lines (at 612.2, 616.2 and 643.9 nm) which have line strengths between 30 mÅ (Ca I 612.2 in the TOP stars) and 92 mÅ (Ca I 616.2 in the RGB stars). The titanium abundances (*bottom*) were determined from the only available ionized line (Ti II 522.6 nm) which has line strengths between 22 mÅ (TOP) and 67 mÅ (RGB). For the relative abundance trends errors of 0.05 are adopted. The observed trends (markedly shallower than for iron) are in good agreement with the diffusion predictions (full-drawn line; the dashed line indicates the original abundances used in the model). Trends were observed for other elements (e.g. scandium, magnesium), but no model predictions exist for some (e.g. scandium) and others (e.g. magnesium, aluminium) suffer from suspected nuclear processing in globular clusters¹⁶ and are thus not suitable for isolating the diffusion signature.

Spectroscopic versus photometric effective temperatures of the four groups of stars observed

Group	No. of stars	$T_{\text{eff}}(\text{spec})$ (K)	$T_{\text{eff}}(v - y)$ (K)	$T_{\text{eff}}(V - I)$ (K)
TOP	5	6254 ± 9	6240 ± 21	6133 ± 31
SGB	2	5805 ± 7	5824 ± 6	5688 ± 8
bRGB	5	5456 ± 57	5408 ± 37	5318 ± 29
RGB	6	5130 ± 19	5132 ± 22	5063 ± 20

Table 2: The photometric indices are calibrated on the infrared-flux method²⁸. The agreement between spectroscopy and $(v - y)$ is excellent, whereas $(V - I)$ is offset towards cooler effective temperatures by roughly 100 K. However, for the identification of the diffusion signature the effective-temperature difference is the most relevant quantity. The effective-temperature difference between TOP and RGB stars in $(V - I)$ is lower than in the other two cases (by roughly 50 K). Because of this, a slightly larger abundance difference would result when referring to the $(V - I)$ temperature scale. The conclusion is that three prominent effective-temperature scales ($H\alpha$ spectroscopy, Strömgren and broad-band photometry) reveal significant abundance differences between the TOP and RGB stars of NGC 6397.